Integer and fractional quantum hall effects in lattice magnets
Venderbos, J.W.F.

Citation
Venderbos, J. W. F. (2014, March 25). *Integer and fractional quantum hall effects in lattice magnets*. *Casimir PhD Series*. Retrieved from https://hdl.handle.net/1887/24911

Cover Page

The handle http://hdl.handle.net/1887/24911 holds various files of this Leiden University dissertation.

Author: Venderbos, Jörn Willem Friedrich
Title: Integer and fractional quantum hall effects in lattice magnets
Issue Date: 2014-03-25

CHAPTER 6

t_{2g} TRIANGULAR LATTICE SYSTEMS

6.1 Introduction

The Integer Quantum Hall (IQH) effect [75] is a prime example of an electronic state that cannot be classified within the traditional framework of symmetry breaking, but is instead characterized by a topological invariant [16]. It is by now theoretically well established that an external magnetic field is in principle not needed and that states within the same topological class as IQH states can be realized in lattice models, if time-reversal symmetry is broken by other mechanisms, e.g., by complex electron hoppings [76]. Related topologically nontrivial Quantum Spin-Hall (QSH) states even occur in systems where time-reversal symmetry is not broken at all [1, 3, 4, 72, 127], see Refs. [12, 111] for reviews. At present, many intriguing features intrinsic to topologically non-trivial states have been observed in the absence of magnetic fields, such as the metallic Dirac cones at the surface of a topological insulator [74, 128], or the QSH effect in quantum wells [6, 112].

Fractional Quantum Hall (FQH) states [10] are topological states that can be seen as composed of quasi-particles carrying an exact fraction of the elementary electronic charge [114]. Apart from the fundamental interest in observing a quasi-particle that behaves in many ways like a fraction of an electron, some FQH states also have properties relevant to fault-tolerant quantum computation [129]. Very recently [87,
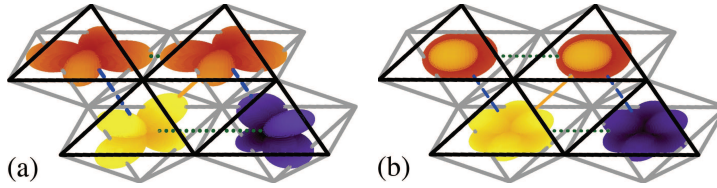
Figure 6.1: Triangular perovskite lattice and t_{2g} orbitals. Oxygen octahedra are indicated by lines, with black lines illustrating the front facets. Thick dotted (dashed, solid) lines indicate nearest-neighbor bonds along lattice vector $\mathbf{a}_1$ ($\mathbf{a}_2$, $\mathbf{a}_3$). (a) Shows two d_{xy} orbitals (top) and one d_{xz} and d_{yz} orbital (bottom). In (b), the orbitals reflecting the three-fold lattice symmetry are shown: The two e'_g orbitals (bottom), which differ by their complex phases, will turn out to be half filled, while the a_{1g} orbital (pointing out of the plane, see top) forms nearly flat bands with non-trivial topological character that can support spontaneous FQH states.

108, 113], it was suggested that lattice-FQH states [115] may similarly arise without a magnetic field, in fractionally filled topologically nontrivial bands.

In contrast to the IQH and QSH effects, which can be fully understood in terms of non-(or weakly-)interacting electrons, interactions are an essential requirement for FQH states, which places demanding restrictions on candidate systems: One needs a topologically nontrivial band that must be nearly flat – similar to the highly degenerate Landau levels – so that the electron-electron interaction can at the same time be large compared to the band width and small compared to the gap separating it from other bands [87, 108, 113]. If the requirements can be fulfilled, however, the temperature scale of the FQH state is set by the energy scale of the interaction. This can allow temperatures considerably higher than the sub-Kelvin range of the conventional FQH effect, which would be extremely desirable in view of potential quantum-computing applications.

In all recently proposed model Hamiltonians [87, 106, 108, 113, 130, 131], the topological nature of the bands was introduced by hand and model parameters were carefully tuned to obtain very flat bands. On the other hand, topologically nontrivial bands can in principle emerge spontaneously in interacting electron systems [84], e.g., for charge-ordered systems [132] or for electrons coupling to spins in a non-coplanar magnetic order [78, 133]. We demonstrate here that such a scenario indeed arises in a Hubbard model describing electrons with a t_{2g} orbital degree of freedom on a triangular lattice: a ground state with topologically nontrivial and nearly flat bands is stabilized by onsite Coulomb interactions, and upon doping the flat bands, longer-range Coulomb repulsion induces a FQH state.

6.2 t_{2g} orbitals on the triangular lattice

The building blocks of our system are oxygen octahedra with a transition-metal (TM) ion in the center, the most common building block in the large and versatile material class of TM oxides. In this case the local symmetry around a TM ion is cubic, with ligand oxygens forming an octahedron, as depicted in Fig. 6.2(a). This splits the degeneracy between the d levels, because the two e_g orbitals point toward the negatively charged oxygens, while the three t_{2g} levels have their lobes in between. Consequently, the energy of e_g levels is higher. Depending on the total electron filling, the valence states may be found in either manifold. We are here discussing the situation where the three t_{2g} levels share 2.5 to 3 electrons and the e_g levels are empty. Furthermore, we consider the case of a layered triangular lattice, as can be realized in compounds of the form ABO_2.

In this geometry, the octahedra are edge sharing and electrons (or holes) can hop from one TM ion to its neighbor either through direct overlap or via the ligand oxygens. The hopping symmetries can be most easily worked out using the usual basis functions for the t_{2g} states, $|xz\rangle$, $|yz\rangle$, and $|xy\rangle$ [124, 125] and following Refs. [134, 135]. Considering hopping for bonds along the $\vec{a}_1$ direction and choosing the local coordinate system such that this corresponds to the $(1, 1)$ direction in the x-y plane, one finds that direct hopping t_d is only relevant for the xy orbital and conserves orbital flavor. Due to the $90°$ angle of the TM-O-TM bond, oxygen-mediated hopping t_0 is, on the other hand, mostly via the oxygen-p_z orbital and mediates processes between xz and yz states, thereby always *changing* orbital flavor. Hoppings along the other two, symmetry-related, directions $\vec{a}_2$ and $\vec{a}_3$ are obtained by symmetry transformations.

These hoppings can then be expressed in orbital- and direction- dependent matrix elements $t_{\vec{a}_j}^{\alpha, \beta}$, where α and β denote orbitals (xz, yz, and xy) and $\vec{a}_j$ the direction. They are given by

$$\hat{T}_{\vec{a}_1} = \begin{pmatrix} t_{dd} & 0 & 0 \\ 0 & 0 & t_0 \\ 0 & t_0 & 0 \end{pmatrix}, \ \hat{T}_{\vec{a}_2} = \begin{pmatrix} 0 & 0 & t_0 \\ 0 & t_{dd} & 0 \\ t_0 & 0 & 0 \end{pmatrix},$$

$$\hat{T}_{\vec{a}_3} = \begin{pmatrix} 0 & t_0 & 0 \\ t_0 & 0 & 0 \\ 0 & 0 & t_{dd} \end{pmatrix} \tag{6.1}$$

for NN bonds along the three directions $\vec{a}_1$, $\vec{a}_2$, $\vec{a}_3$. The two hopping processes are expected to be of comparable strength, but with $|t_d| \lesssim |t_0|$ for $3d$ elements, and will typically have opposite sign. [125]

If the width of a triangular layer made of octahedra is compressed (extended), the energy of the highly symmetric orbital state $|a_{1g}\rangle = (|xz\rangle + |yz\rangle + |xy\rangle)/\sqrt{3}$ is

raised (lowered) with respect to the remaining orbital doublet (e'_g), see Fig. 6.2(b) for illustration. This energy shift can be written as

$$\hat{H}_{\text{JT}} = -\Delta_{\text{JT}}(\hat{n}_{e_{g+}} + \hat{n}_{e_{g-}} - 2\hat{n}_{a_{1g}})/3 \tag{6.2}$$

and depends on the Jahn-Teller effect as well as on the lattice. [125] Especially for large splitting between a_{1g} and e'_g states, which may also be enhanced through on-site Coulomb interactions, see Section 6.3 and also 7.2, it is more appropriate to use a basis that reflects the triangular lattice symmetry. We thus go over into the $(a_{1g}, e'_{g,1}, e'_{g,2})$ basis, which is done via [125]

$$\begin{pmatrix} a_{1g} \\ e'_{g,1} \\ e'_{g,2} \end{pmatrix} = \hat{U} \begin{pmatrix} xz \\ yz \\ xy \end{pmatrix} = \frac{1}{\sqrt{3}} \begin{pmatrix} 1 & 1 & 1 \\ 1 & e^{i2\pi/3} & e^{-i2\pi/3} \\ 1 & e^{i4\pi/3} & e^{-i4\pi/3} \end{pmatrix} \begin{pmatrix} xz \\ yz \\ xy \end{pmatrix}. \tag{6.3}$$

The transformed hopping matrices $\widetilde{T}_{\vec{a}_i}$ are then obtained from Eq. (6.1) as

$$\widetilde{T}_{\vec{a}_1} = \hat{U}^\dagger \hat{T}_{\vec{a}_1} \hat{U} = \frac{1}{3} \begin{pmatrix} 3t_0 + \delta t & \delta t & \delta t \\ \delta t & \delta t & 3t_0 + \delta t \\ \delta t & 3t_0 + \delta t & \delta t \end{pmatrix},$$

$$\widetilde{T}_{\vec{a}_2} = \hat{U}^\dagger \hat{T}_{\vec{a}_2} \hat{U} = \frac{1}{3} \begin{pmatrix} 3t_0 + \delta t & \delta t\,\omega & \delta t\,\omega^{-1} \\ \delta t\,\omega^{-1} & \delta t & (3t_0 + \delta t)\omega \\ \delta t\,\omega & (3t_0 + \delta t)\omega^{-1} & \delta t \end{pmatrix},$$

$$\widetilde{T}_{\vec{a}_3} = \hat{U}^\dagger \hat{T}_{\vec{a}_3} \hat{U} = \frac{1}{3} \begin{pmatrix} 3t_0 + \delta t & \delta t\,\omega^{-1} & \delta t\,\omega \\ \delta t\,\omega & \delta t & (3t_0 + \delta t)\omega^{-1} \\ \delta t\,\omega^{-1} & (3t_0 + \delta t)\omega & \delta t \end{pmatrix}, \tag{6.4}$$

where $\delta t = t_{dd} - t_0$ and $\omega = e^{i2\pi/3}$. Observe that the intra-orbital hopping of the a_{1g} state is the same in all three lattice directions, as expected for a_{1g} symmetry. However, we also see that hopping elements mix all three orbitals. We set here $n < 3$ and choose $t > 0$ [125] as unit of energy, but analogous results hold for $n > 3$, $t < 0$, and $t_{dd} \to -t_{dd}$, $\Delta_{\text{JT}} \to -\Delta_{\text{JT}}$ due to particle-hole symmetry.

6.3 Multi-orbital interacting model

In TM oxides, Coulomb interaction is substantial compared to the kinetic energy of t_{2g} orbitals and spin-orbital physics induced by correlations are known to be rich in t_{2g} systems on triangular lattices [124, 136]. We take into account the onsite inter-action including Coulomb repulsion U (intra-orbital) and U' (interorbital) as well as
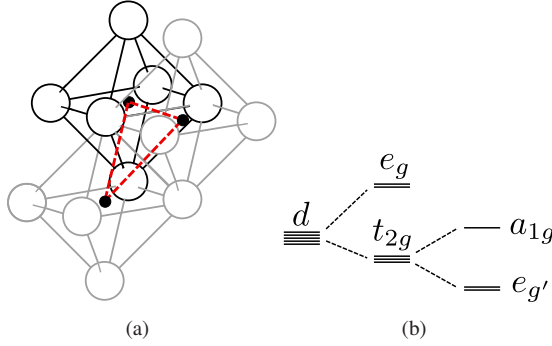
Figure 6.2: (a) Illustration of a triangular-lattice plane built of edge-sharing oxygen octahedra. (b) The five d orbitals of the transition-metal ion in the center are split into an e_g doublet and a t_{2g} triplet due to the local cubic symmetry; the latter is further split into one a_{1g} state and an e_g' doublet. (The splitting between the latter is exaggerated here for visibility.)

Hund's-rule coupling J. The Hamiltonian corresponding to the kinetic energy of the t_{2g} electrons is given by

$$\hat{H}_{\text{int}} = \sum_{ij,\alpha\beta} t_{ij}^{\alpha\beta} \hat{\psi}_{i\alpha\sigma}^{\dagger} \hat{\psi}_{j\beta\sigma} + \text{hc} \tag{6.5}$$

where the matrix $t_{ij}^{\alpha\beta}$ depends on the direction and orbital flavor and is constructed from the previously explicitly defined $\widetilde{T}_{\vec{a}_i}$. The full Coulomb interaction interaction for equivalent t_{2g} orbitals reads

$$\hat{H}_{\text{int}} = U \sum_{i,\alpha} \hat{n}_{i\alpha\uparrow}\hat{n}_{i\alpha\downarrow} + (U' - J/2) \sum_{i,\alpha<\beta} \hat{n}_{i\alpha}\hat{n}_{i\beta} - 2J \sum_{i,\alpha<\beta} \vec{s}_{i\alpha} \cdot \vec{s}_{i\beta}$$

$$+ J' \sum_{i,\alpha<\beta} \left(\hat{\psi}_{i\alpha\uparrow}^{\dagger}\hat{\psi}_{i\alpha\downarrow}^{\dagger}\hat{\psi}_{i\beta\downarrow}\hat{\psi}_{i\beta\uparrow} + \text{hc} \right) \tag{6.6}$$

where $U = U' + 2J$ and $J' = J$ holds in the case of equivalent t_{2g} orbitals. The spin operators $\vec{s}_{i\alpha}$ are defined as

$$\vec{s}_{i\alpha} = \hat{\psi}_{i\alpha\sigma}^{\dagger}\vec{\sigma}_{\sigma\sigma'}\hat{\psi}_{i\alpha\sigma'}. \tag{6.7}$$

We concentrate on the regime of interest, where the a_{1g} orbital is separated from the e_g doublet by a sizable Δ_{JT} and does not have to be equivalent. As long as intraor-

bital interaction (controlled by U) and Hund's rule coupling (controlled by J) dominate over interorbital interaction ($U' - J/2$) and crystal-field splitting (Δ), doubly occupied orbitals will be suppressed and the last term in Eq. (6.3) will consequently not be important and hence neglected.

To study the magnetic and ordbital ordering of these t_{2g} orbitals on the triangular lattice we employ a mean-field approximation with a decoupling into expectation values of densities $\langle \hat{n}_{i\alpha\sigma} \rangle = \langle \hat{\psi}^{\dagger}_{i\alpha\sigma} \hat{\psi}_{i\alpha\sigma} \rangle$ for site i, orbital α, and spin σ [30,137]. For the interacting term $\vec{s}_{i\alpha} \cdot \vec{s}_{i\beta}$ the fact that we only keep densities has the consequence that

$$-2J \sum_{i,\alpha<\beta} \vec{s}_{i\alpha} \cdot \vec{s}_{i\beta} \;\rightarrow\; -2J \sum_{i,\alpha<\beta} \hat{s}^{z}_{i\alpha} \hat{s}^{z}_{i\beta}. \tag{6.8}$$

This apparent breaking of $SU(2)$ invariance can be restored by defining the spin quantization axis locally. The fact that the spin-quantization axis is not the same at all sites implies that the hopping no longer conserves the new spin. Instead, hopping acquires as spin-dependent factor $t^{\alpha\beta}_{ij} \rightarrow t^{\alpha\beta\sigma\sigma'}_{ij} = t^{\alpha\beta}_{ij} u^{\sigma\sigma'}_{ij}$, [28] with

$$u^{\uparrow\uparrow}_{ij} = c_i c_j + s_i s_j e^{-i(\phi_i - \phi_j)}, \tag{6.9}$$
$$u^{\downarrow\downarrow}_{ij} = c_i c_j + s_i s_j e^{i(\phi_i - \phi_j)}, \tag{6.10}$$
$$u^{\sigma\bar{\sigma}}_{ij} = \sigma(c_i s_j e^{-i\sigma\phi_j} - c_j s_i e^{-i\sigma\phi_i}),$$

where $\bar{\sigma} = -\sigma$ and $c_i = \cos\theta_i/2$, $s_i = \sin\theta_i/2$ and the set of angles $\{\theta_i\}$ and $\{\phi_i\}$ are the polar and azimuthal angles corresponding to $\{\vec{s}_i\}$, respectively. As one can see, these effective hoppings can become complex, and it has been shown that non-coplanar spin configurations can endow the electronic bands with a nontrivial topology. [30,85] Additionally, the itinerant electrons mediate an interaction between the localized spins, which typically competes with antiferromagnetic spin-spin interactions; on frustrated lattices, this competition can resolve itself in non-coplanar – and thus topologically nontrivial – phases [30–32,100]. There is no reason for spins in different orbitals, but on the same site, to point in different directions, as the only interactions between spins are FM, i.e., we can use the same local quantization axis for all orbitals, which is why we decomposed $t^{\alpha\beta}_{ij} \rightarrow t^{\alpha\beta}_{ij} u^{\sigma\sigma'}_{ij}$. In the case of doubly occupied orbitals, one spin can be seen as lying antiparallel and from now on "↑" ("↓") denotes a spin parallel (antiparallel) to the local quantization axis.

The mean-field decoupling then takes the specific form

$$U \sum_{i,\alpha} \hat{n}_{i\alpha\uparrow} \hat{n}_{i\alpha\downarrow} \rightarrow U \sum_{i,\alpha} \langle \hat{n}_{i\alpha\uparrow} \rangle \hat{n}_{i\alpha\downarrow} + \hat{n}_{i\alpha\uparrow} \langle \hat{n}_{i\alpha\downarrow} \rangle - \langle \hat{n}_{i\alpha\uparrow} \rangle \langle \hat{n}_{i\alpha\downarrow} \rangle$$

$$(U' - \frac{J}{2}) \sum_{i,\alpha<\beta} \hat{n}_{i\alpha} \hat{n}_{i\beta} \rightarrow (U' - \frac{J}{2}) \sum_{i,\alpha<\beta} \langle \hat{n}_{i\alpha} \rangle \hat{n}_{i\beta} + \hat{n}_{i\alpha} \langle \hat{n}_{i\beta} \rangle - \langle \hat{n}_{i\alpha} \rangle \langle \hat{n}_{i\beta} \rangle$$

$$-2J \sum_{i,\alpha<\beta} \hat{s}_{i\alpha}^z \hat{s}_{i\beta}^z \rightarrow -2J \sum_{i,\alpha<\beta} \langle \hat{s}_{i\alpha}^z \rangle \hat{s}_{i\beta}^s + \hat{s}_{i\alpha}^z \langle \hat{s}_{i\beta}^z \rangle - \langle \hat{s}_{i\alpha}^z \rangle \langle \hat{s}_{i\beta}^z \rangle \qquad (6.11)$$

Due to the last term Eq. (6.3), an electron in orbital β feels a FM coupling to a "classical localized spin" with length $\sum_{\alpha\neq\beta} \langle \hat{s}_{i\alpha} \rangle$ that points along the local quantization axis.

6.4 Mean field phase diagram

We use numerical optimization routines to find the spin pattern with the lowest energy among all orderings with unit cells of up to four sites, including all patterns considered in Ref. [31] of the main text. We search for mean-field solutions which break translational symmetry such that the unit cell is either tripled or quadrupled. In each step, the mean-field energy is calculated self-consistently for a lattice of 16×16 (four-site unit cell) or 24×16 (three-site unit cell). (For selected points in parameter space, we also used larger lattices and did not find a significant difference.) In order to minimize the impact of our approximations on the symmetries of the orbital degrees of freedom, we perform the mean-field decoupling in the $\{a_{1g}, e'_{g+}, e'_{g-}\}$ basis, where the symmetry between the half-filled e'_{g+} and the quarter-filled a_{1g} orbitals (for the fillings discussed here) is already broken by the crystal field. We verified that decoupling directly in the $\{xy, xz, yz\}$ basis, where all three orbitals have the same electronic density, leads to qualitatively identical and quantitatively very similar results.

For simplicity, we present here results for $J/U = 1/4$ and the relation $U' = U - 2J$ between the Kanamori parameters was used, but we have verified that the results presented remain robust for other choices.

For wide parameter ranges (see below), the ground state is the non-coplanar spin-chiral phase illustrated in Fig. 6.4(a,b). As demonstrated in the context of the Kondo-lattice model [30, 31], this magnetic order leads to topologically nontrivial bands, which can also be seen in the one-particle bands shown in Fig. 6.4(c). The chemical potential lies within the a_{1g} states of the lower Hubbard band, where the electron spin is mostly parallel (labelled by $\uparrow$) to the direction defined by the spin-chiral pattern.

(a)

(b)
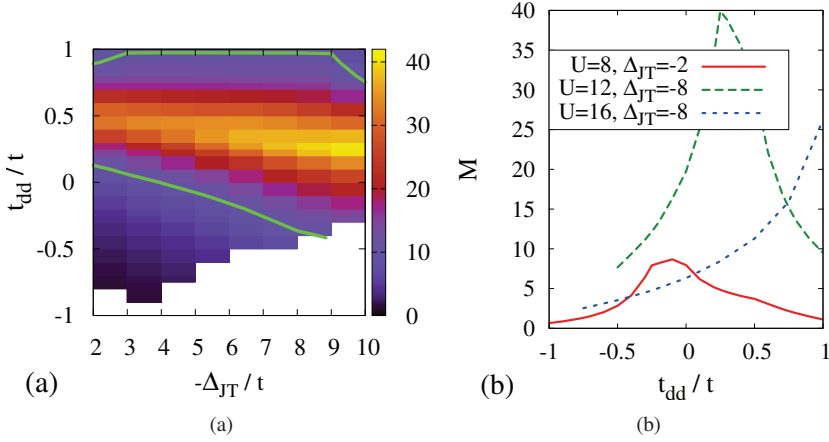
Figure 6.3: Stability of the spin-chiral phase and flatness of the topological bands depending on parameters of the Hamiltonian. In (a), shaded areas in the t_{dd}-Δ_{JT} plane indicate a spin-chiral ground state Fig. 6.4(a,b) for $U/t = 12$, white areas have a different ground state. Shading indicates the figure of merit M for the flatness of the upper chiral subband, bright thick lines bound the region with $M \geq 10$. (b) shows M depending on t_{dd} for selected sets of U and Δ_{JT}. Where the "Mott gap", which separates the flat topologically non-trivial band from the upper Hubbard band, becomes very small, M is determined by the minimal gap separating the band of interest from other bands. $J = U/4$ and $t = 1$ were used in all cases.

Dashed and dotted lines decorate states living on the top and bottom edges of a cylinder, they cross the chiral gap exactly once as one left- and one right-moving edge mode, indicating the different Chern numbers associated with the two bands directly above and below the chemical potential.

Figure 6.4(c) also indicates that the upper chiral subband has a very small width, ~ 14 times smaller than the chiral gap. One can quantify the band flatness by a figure of merit M given by the ratio of the gap to the band width. Its dependence on various parameters of the Hamiltonian is shown in Fig. 6.3. It peaks at $M > 40$, but the more striking observation is that it is above 5 or even 10 for wide ranges of U, Δ_{JT} and t_{dd}, in contrast to many other proposals that require carefully fine-tuned parameters [87, 104, 106, 108, 113, 130, 131]. Nearly flat chiral bands are thus very robust in this system and both their topological character and their flat dispersion emerge spontaneously with purely onsite interaction and short-range hopping, without spin-orbit
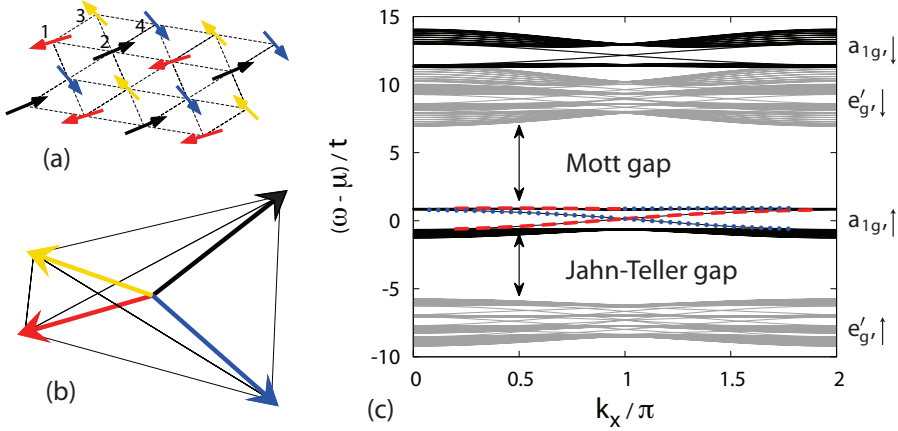
Figure 6.4: (Color online) Spin-chiral magnetic phase with topologically nontrivial bands stabilized by onsite Coulomb interactions in t_{2g} electrons on a triangular lattice. (a) Chiral magnetic order, the sites of the unit cell are labeled by 1 to 4. (b) The spins on the four sites can be seen as pointing to the corners of a tetrahedron, i.e., the pattern is non-coplanar. (c) One-particle energies on a cylinder (periodic boundary conditions along x) in the mean-field ground state of the t_{2g} multiorbital Hubbard model, which is given by the pattern shown in (a). States drawn in black (grey) have more (less) than 33% a_{1g} character, dashed and dotted lines indicates edge states with more than 33% of their weight on the top (bottom) row of sites. The arrows $\uparrow$ ($\downarrow$) indicate states with electron spin mostly (anti-)parallel to the local quantization axis, which can be seen as the lower (upper) Hubbard band. The filling is 2.5 electrons per site, slightly less than half filling. Parameters used were $t = 1$, $t_{dd} = 0$, $U/t = 12$, $J/t = 3$, $\Delta_{\mathrm{JT}}/t = -6$. The figure of merit M, which is given by the ratio of the gap separating the two a_{1g} subbands of the lower Hubbard band and the band width of the highest subband of the lower Hubbard band, is $M \approx 14$.

coupling or any explicit breaking of time-reversal symmetry.

In order to understand the origin of the spin-chiral state, it is helpful to look at the one-band Kondo-lattice model (KLM), which describes itinerant electrons coupled to localized spins. The KLM supports spin-chiral phases because of frustration between ferromagnetism (driven by double exchange, i.e., the kinetic energy of the electrons) and antiferromagnetism (driven by superexchange between the localized spins) on many frustrated lattices like the triangular [30–32, 100], pyrochlore [33], and face-centered cubic [29] lattices. Our model can be related to the KLM by noting that the half-filled e'_g levels are far from the chemical potential and act as a localized spin to which the electrons in the a_{1g} orbital are coupled via Hund's rule coupling. The anti-ferromagnetic superexchange arises through excitations into the upper Hubbard band. Consequently, it is suppressed by a larger Mott gap and the ground state becomes fer-romagnetic for $U \gtrsim 24|t|$, as in the KLM with a large Kondo gap [31, 100]. In a large window $6 \lesssim U/|t| \lesssim 24$, the balance of kinetic energy and superexchange stabilizes a spin-chiral ground state and flat bands with $M > 5$ are found for a window of $8 \lesssim U/|t| \lesssim 20$.

Finally, we note that the fact that onsite interactions U and J are only large, but *not* infinite, is important for the spin-chiral ground state: For very large U and J, the ground state becomes a ferromagnet. [107] This can be related to the fact that the Kondo-lattice model requires either finite J_{Kondo} [31] or additional AFM inter-site superexchange [32] to support a spin-chiral instead of a FM state. At finite onsite in-teractions, virtual excitations with doubly occupied e'_g orbitals are possible and lead to second-order processes that are similar to the effective longer-range hoppings dis-cussed above. In such a process, an e'_g electron hops into an occupied e'_g state at a NN site, creating a (virtual) intermediate state with energy $\propto U + J \approx U' + 3J$, and hops back in the next step. Such a process yields an energy gain $\propto t^2_{e'_g}/(U + J)$ and is only possible if the spins of the two involved electrons, which occupy the same or-bital in the intermediate state, are opposite. The mechanism thus effectively provides the needed AFM intersite superexchange and the spin-chiral state becomes stable for wide parameter regimes, including ranges supporting nearly flat upper chiral sub-bands. [107]

6.5   Conclusions

The possibility of a spontaneous FQH effect without a magnetic field is currently intensely discussed, and various models have been suggested [87, 104, 106, 108, 113, 130, 131]. In these proposals, the necessary topological character of the bands was introduced by hand, the flatness of the bands needed fine-tuning and the underlying lattices were often rather exotic; an experimental realization appears therefore chal-

lenging. We have shown here that in strongly correlated t_{2g} orbitals on a triangular lattice, bands with the desired properties emerge spontaneously for wide parameter ranges and support FQH ground states. Both t_{2g} systems and triangular lattices occur in various TM oxides, and signatures of the unconventional *integer* QH state have been reported for a triangular-lattice palladium-chromium oxide [80]. This harbors the prospect that a suitable material can be synthesized in this highly versatile material class. As such a material is by default strongly correlated, one also naturally expects an inter-site Coulomb repulsion that is strong enough to stabilize spontaneous FQH states in the absence of a magnetic field.